Int J Fract (2011) 170:183–190
DOI 10.1007/s10704-011-9608-8
© Springer Science+Business Media B.V. 2011

LETTERS IN FRACTURE AND MICROMECHANICS

MICROMECHANICAL MODELING AND NUMERICAL SIMULATION OF CHAIN-MAIL ARMOR

G. N. Mseis and T. I. Zohdi
Department of Mechanical Engineering
6195 Etcheverry Hall
University of California, Berkeley, CA, 94720-1740, USA
email: mseis@berkeley.edu, zohdi@newton.berkeley.edu

Abstract. The microstructure of chain-mail (CM) armor consists of a network of small links that are connected together to form a sheet. A network-type model, amenable to straightforward numerical simulation, is formulated, where the links are modeled as supporting only axial (tensile) loading, and where the interconnections are idealized as three-dimensional frictionless pin-joints. Because of its use as a ballistic shield, the strain-rate dependent thermo-mechanical (viscoplastic) response is important, due to thermal softening. The philosophy behind the proposed direct modeling approach is to harness the dramatic increases in readily available scientific computing to simulate realistic responses of structural CM, by starting directly at the microscale, where relatively simple description of the material is possible. By employing enough of these simple structural elements, one can build an entire macroscale sheet of CM. The deformation of the CM is dictated by solving a ("link-coupled") system of differential equations for the motion of the interconnected masses. Large-scale simulations, illustrating the thermomechanical response of chain-mail material armor, undergoing impact with a rigid indenter, are presented to illustrate the potential of the approach in delivering realistic responses, involving dynamic rupture and penetration of structural CM.

1 Introduction. We consider materials with microstructures known as "chain-mail" (CM) armor that is made from chain or chain links, woven together to form a flexible "metal fabric". Since chain-mail is intended to protect against concentrated impact by redistributing the load in the contact zone, we concentrate on blunt impactors. There are many types of CM, all of which have a basic common underlying structure, namely, chain links that are connected together to form networks of chains and, ultimately, sheets. These patterns can be quite elaborate, however, in this paper we will concentrate on the most basic rectangular grid-like structure (Figure 1). The structure can be idealized as a network of small pinned-end links that take purely axial tensile loading, and nothing in compression (since the links slide relative to one another in compression). A key aspect of our approach is that if the properties of the links are known, the structural scale (sheet-level) properties can be constructed, without resorting to phenomenological parameters. For most types of structural CM, the overall rupture of a single link is gradual, as opposed to abrupt, due to plastification within the links. An important feature of the direct modeling approach is the ability to directly incorporate the plastification and rupture of each metallic link into the structural scale response of the CM.

A reduced-order model is constructed by combining a link-network representation with dynamic discrete/lumped masses. The deformation of the CM is dictated by solving a coupled system of differential equations for the motion of the lumped masses, which are coupled through the links. Quantitative numerical simulations are provided for the entire,

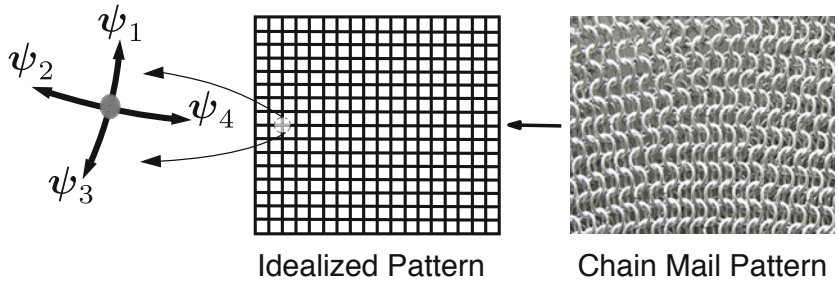

Figure 1: A network representation linked segments, joined together by pin-joints to form a network, and the mass of the material are lumped at the connection points.

assembled, larger-scale, coupled system, based on a computationally-efficient time-stepping algorithm. The model is relatively easy to implement and provides analysts with a straightforward tool to study such systems. This type of modeling extends previous works on ballistic fabric shields, found in Zohdi [1] and Zohdi and Powell [2]. For a general introduction to fabric modeling, the reader is referred to Shim *et al* [3], Cheeseman and Bogetti [4], Duan *et al* [5, 6, 7], Tan *et al* [8] and a review article by Tabiei and Nilakantan [9].

2 Modeling of links. Due to the fact that the links represent chain-links, we assume that the compressive response of the CM is insignificant, in particular, since the CM will be carrying overall tensile loading as a shield. Explicitly, we enforce a zero stress state for any compressive strains; a so-called "relaxed model". The analysis of relaxed models dates back to Buchholdt *et al* [10], with an extensive analysis found in Atai and Steigmann [11, 12]. Relaxed formulations have served as a foundation for more elaborate models describing rupture of ballistic fabric shielding in Zohdi [1, 13] and Zohdi and Powell [2], and are the basis for the present approach. The following simplifying assumptions are made: (1) the links are quite thin, therefore one may assume a uniaxial-stress type condition (the forces only act along the length of the link and remain straight, undergoing a homogeneous stress state), (2) the link-segments are pin-joined at the nodes, producing no moments, (3) the link buckling is ignored and (4) the masses of the links are represented by discrete lumped masses whose locations coincide with those of the pin-joints. With these assumptions, the response can be described by a simple constitutive model such that the stored energy in a single link is $W = \frac{1}{2}\mathbb{E}(E - E_p)^2$, where $\mathbb{E}$ is Young's modulus and E is the total Green-Lagrange strain and E_p is the plastic strain. The corresponding Second Piola-Kirchhoff stress is $S = \mathbb{E}(E - E_p)$. Recalling that the Cauchy stress can be related to the second Piola-Kirchhoff stress by $\sigma = \frac{1}{J}FSF = FS$, we now define the plastic flow rule in one-dimension as, (a) $\dot{E}_p = 0$, if $\sigma \leq \sigma_y$ and (b) $\dot{E}_p = a\left(\frac{\sigma}{\sigma_y} - 1\right)$ if $\sigma > \sigma_y$. Where σ_y is the Cauchy yield stress. The constant, a, is the flow rule modulus and it is a user defined parameter. We also assume that the yield stress has a temperature dependence defined as, $\sigma_y = \sigma_{y0} + d\left(1 - \frac{\theta}{\theta_0}\right)$. Where σ_{y0} is the initial yield stress, θ_0 is the initial temperature of the CM sheet and θ is the current temperature. The parameter, d, is also a user defined constant that determines the degree of dependency the yield stress has on the temperature. We note from the balance of linear momentum we have $m\ddot{\mathbf{r}}_i = \boldsymbol{\psi}_i^{ext} + \sum_{I=1}^{4} \boldsymbol{\psi}_{iI}$, where $\boldsymbol{\psi}_{iI}$ are the internal forces in the links, $\boldsymbol{\psi}_i^{ext}$ can be any external loading, such as contact forces

and m is the lumped mass. A more detailed description of the mechanical lumping is found in Zohdi [1] and Zohdi and Powell [2].

2.1 Thermodynamic lumping. The thermodynamic model extends the use of the lumped mass assumption utilized in Zohdi [1] and Zohdi and Powell [2]. To derive this response, we start by considering the local form of the 1st law of thermodynamics in the reference configuration which is stated as

$$\rho_0 \dot{w} = S\dot{E} - \nabla_{\mathbf{X}} \cdot \mathbf{Q} \tag{1}$$

where ρ_0 is the reference density, $S\dot{E}$ is the stress power, $\mathbf{Q}$ is heat flux in the reference configuration and $\dot{w}$ is the internal power. In addition $\nabla_{\mathbf{X}} \cdot ()$ is the divergence operator with respect to reference coordinates $\mathbf{X}$. We start by assuming a form on the internal power as

$$\rho_0 \dot{w} = S(\dot{E} - \dot{E}_p) + \rho_0 c \dot{\theta} \tag{2}$$

with c being the specific heat capacity. It is more natural to consider the definition of the heat flux on the current configuration as $\mathbf{q} = -k\nabla_{\mathbf{x}}\theta$, where k is the thermal conductivity and $\nabla_{\mathbf{x}}()$ is the gradient operator with respect to current coordinates $\mathbf{x}$. Note the relationship between the current and reference configuration fluxes is, $\int_\Omega \mathbf{q} \cdot \mathbf{n} da = \int_{\Omega_0} \mathbf{Q} \cdot \mathbf{N} dA$, where $\mathbf{n}$ and $\mathbf{N}$ are the normals to the surface on the current and reference configurations respectively. We now consider Eqn. 1 and integrate over a region Ω_0 defined by containing one lumped mass surrounded by intersecting links as shown in Figure 2. The resulting form after replacing $\rho_0 \dot{w}$ with the assumed form in Eqn. 2 into Eqn. 1 is, $\int_{\Omega_0} \rho_0 c \dot{\theta} dV = \int_{\Omega_0} \left(S\dot{E}_p - \nabla_{\mathbf{X}} \cdot \mathbf{Q} \right) dV$. Applying the divergence theorem we obtain and using the relation between the reference and current configuration fluxes we have, $\int_{\Omega_0} \rho_0 c \dot{\theta} dV = \int_{\Omega_0} S\dot{E}_p dV - \int_\Gamma \mathbf{q} \cdot \mathbf{n} da$.

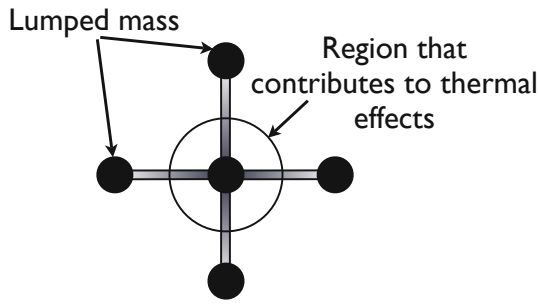

Figure 2: Schematic showing a set of lumped masses. The encircled region indicates that half the plastic work is used for the center mass and the other half for the other masses.

Since we are assuming a lumped mass model, we can integrate the terms explicitly to obtain the form, $mc\dot{\theta} = \sum_{I=1}^{4} \psi_{iI}^{tot}$. Where ψ_{iI}^{tot} is a sum of the flux and the plastic work $(S\dot{E}_p)$ contributions of the Ith link to the ith mass. Since the plastic work is a volume integral over the entire link, to conserve energy, we delegate half the total plastic work to

each mass point it is connected to. Therefore, we have $\psi_{iI}^{tot} = 0.5 S_I \dot{E}_{pI} V_0 + k \nabla_{\mathbf{x}} \theta_I . \mathbf{n}_I A_I$, where A_I is the current cross sectional area of the link, V_0 is the reference volume of the link and the normal along which the heat flux acts is defined as $\mathbf{n}_I = \frac{\mathbf{r}_I^+ - \mathbf{r}_I^-}{||\mathbf{r}_I^+ - \mathbf{r}_I^-||}$ with $\mathbf{r}_I^+$ defined as the endpoint of the link that is not in contact with the mass while $\mathbf{r}_I^-$ is the endpoint in contact with the mass. We note that the plastic work term is what generates heat. For high plastic strain rates this term will be the dominant contribution to ψ^{tot}. Unless the conductivity constant, k, is very large, the flux term will be small for large plastic strain rates.

2.2 Link Damage. To include link damage we consider a model that causes abrupt fracture of the link when a certain value of plastic strain is exceeded. This is simply identified when $E_p > E_p^*$ and then the corresponding link is ruptured and we set $\mathbb{E} = 0$. Note that E_p^* is a user defined limit on the plastic strains. This can be easily included and does not require modifying any of the previously derived equations.

3 Numerical Examples of CM under impact. The coupled system of equations for the mechanical response, the thermodynamic response and the contact are solved using a staggering scheme of which details can be found in Park and Felippa [14], Zienkiewicz [15], Zohdi and Wriggers [16]. A brief overview is presented. The contact algorithm is a simple predictor-corrector method in which the impactor is a rigid body. The algorithm detects if the projectile penetrates the CM sheet and then projects the respective lumped masses onto the closest projectile surface and calculates the amount of force required to achieve this. In turn these contact forces act on the projectile and affect its position, this iterative process is repeated until convergence is achieved, a similar approach to this contact algorithm can be found in Zohdi [17]. The coupling between the mechanical response and the thermodynamic response is achieved, as mentioned, through a staggering scheme, in which the mechanical response is solved while the thermodynamic fields are held constant. The new position vectors and stresses are then input into the thermodynamic equations to update the temperature field, which in turn affects the mechanical response. This interaction is an iterative process and continues until both the thermal and mechanical fields are converged. The discretized equations are stated in an implicit form and solved using a midpoint rule.

With this in mind, we show some numerical results for a CM under impact. The thermomechanical properties of the links are summarized in Table 1 and correspond to Aluminum. We assume a square sheet of dimension $0.076m \times 0.076m$ and a distribution of link per square meter of $y = 1378^2/m^2$. The sheet of CM is assumed to be 0.5mm thick and therefore the lumped mass is $m = 7.0748 \times 10^{-7}$ kg. Given the link per square meter value, we can calculate the number of nodes or lumped masses in the sheet. In this case we have $N = \sqrt{yl^2} + 1 = 105$ nodes, where the length, l, is the dimension of one side of the sheet. The links are assumed to fail when a plastic strain of $E_p^* = 3.0\%$ is reached.

For the ensuing analysis we consider two types of boundary conditions (1) fixed positions along the CM edges and (2) fixed positions on the corners of the CM as shown in Figure 3. A spherical projectile of radius $r_p = 0.00335$m and mass $m_p = 0.0044$kg is used for the analysis. Three different initial projectile velocities are used for the simulations, the set are $v_z = (400, 500, 600)$ m/s with the remaining components set to zero.

Table 1: Chain Mail Link Properties

ρ (kg/m^3)	E (GPa)	σ_y (MPa)	a	d (Pa)	c (J/(kgK))	k (W/(mK))
2700	70	400	100	1×10^6	900	250

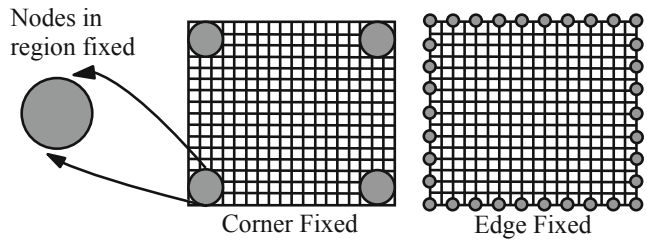

Figure 3: Schematic showing the two types of boundary conditions used. The image on the left shows the corner fixed boundary condition, the image on the right shows the edge fixed case.

3.1 Results: CM with fixed corners. We start with the corner fixed case. Specifically, the corners are fixed with a radius of $r = 0.0027m$. Hence, the displacement of nodes lying in this region are zero. The observed behavior shows that as the CM is stretched the links at the free edges are brought inward and the CM sheet starts expanding out of plane. The temperature contours in the CM prior to failure and the projectile velocity profile is shown in Figure 4. We notice the rise in temperature, hence plastification, is concentrated around the boundary conditions (corners). This is where the chain-mail links fail, and it corresponds to where the greatest temperature increase occurs. We note because of plastification, the trend in the drop of projectile velocity varies depending on the initial projectile velocity. Specifically, the rate in the velocity drop is higher for larger initial velocities. Although, the CM fails for an initial projectile velocity of $v_z = 400$m/s, the projectile in fact is stopped and starts moving with a small negative velocity. In Figure 5 we show the average temperature in the entire sheet and the average temperature in the region of contact for the three different initial projectile velocities. We notice the average temperature in the contact region is higher than that of the entire sheet. This is because although failure occurs at the corners a significant amount of deformation and plastification occurs in the contact region. Additionally, as the projectile speed is increased, the average temperature in the CM increases. We note the temperatures in the CM at the corners with increasing velocity are $\theta_{max} = [543.79, 559.6, 567.9]$ K.

3.2 Results: CM with fixed edges. We now consider the case of fixed edges. In this case we only fix the line of nodes that lie exactly on the edge. Under these boundary conditions, in contrast to the corner fixed case, the CM fails in the region of contact. As the projectile contacts the CM, the sheet of CM balloons outwards until penetration occurs. The results from the simulations are summarized in Figure 6-7 . The average temperature rise in both the contact area and the entire CM are shown in Figure 7. We notice that there is a greater rise in temperature in the contact area then in the overall CM, this is expected since this is where the CM sheet fails. This fact is clearly illustrated in the temperature contour plot in Figure 6. The velocity profile of the projectile for each case is shown in Figure 6. We

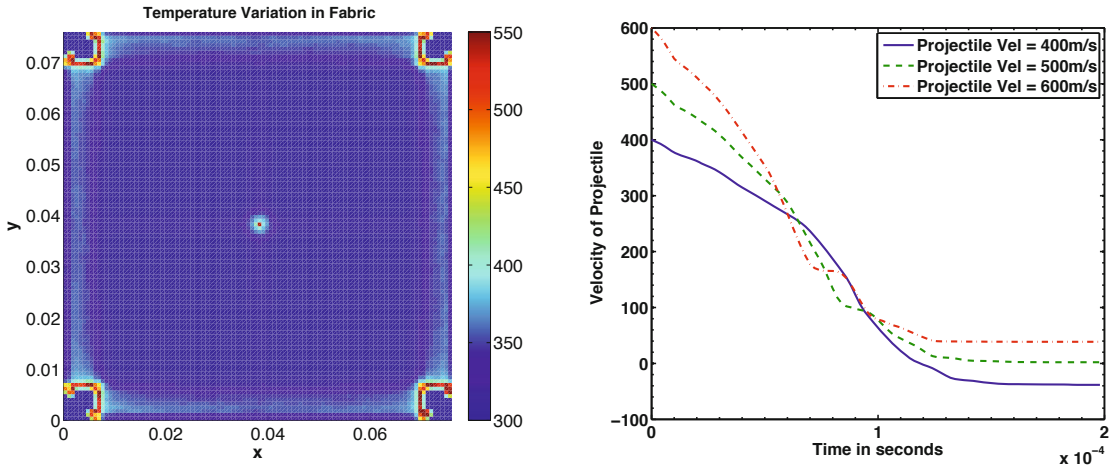

Figure 4: Temperature distribution in corner fixed CM prior to failure for projectile velocity of 600m/s is shown on the left. On the right the various projectile velocity profiles are shown.

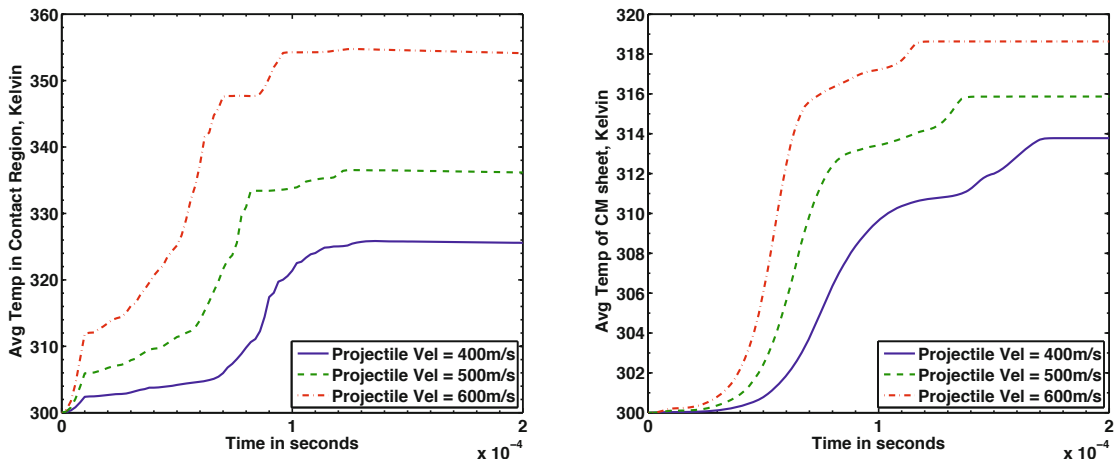

Figure 5: Fixed corner boundary conditions showing the average temperature in the region of contact which is the left plot and the average temperature in the entire CM is the right plot.

again notice that trend in the drop of velocity depends on the initial projectile velocity. This is can be attributed to different amounts of plastification in the CM sheet for the different impact velocities. After penetration the projectile velocity remains constant and does not interact with the CM. Similar to the corner fixed boundary conditions we notice a proportional correlation between the initial projectile velocity and the rise in the average temperature, as shown in Figure 7. We note that under these boundary conditions, the average temperature in the CM keeps rising even after projectile has penetrated the CM sheet. This can be attributed to momentum, where the lumped masses with enough velocity can maintain an increase in plastic strain and thus a maintained rise in temperature. We also note that maximum temperature in the CM sheet with increasing velocity is $\theta_{max} = [606.84, 627.43, 662.05]$ K.

Summary and Conclusions. In this study we have derived a simplified set of equations

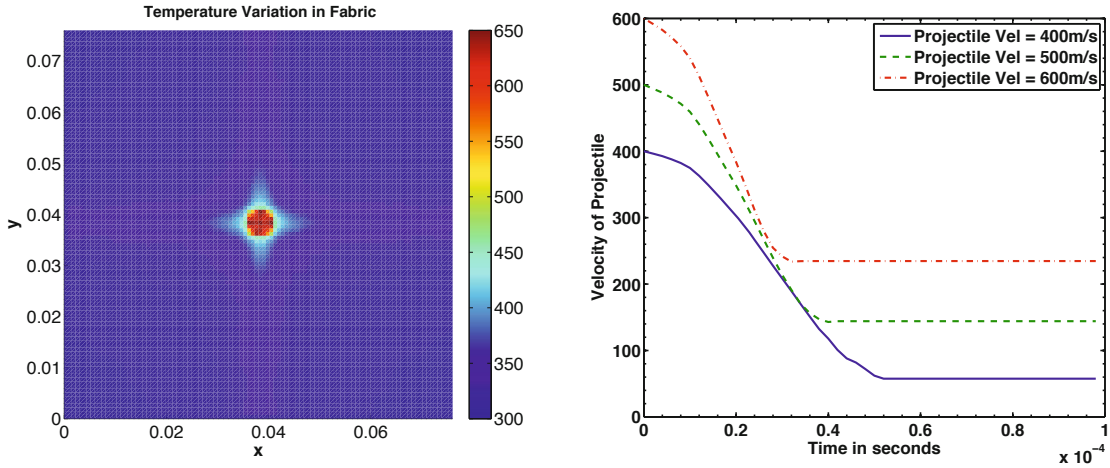

Figure 6: Temperature distribution in edge fixed CM prior to failure for projectile velocity of 600m/s is shown on the left. On the right the various projectile velocity profiles are shown.

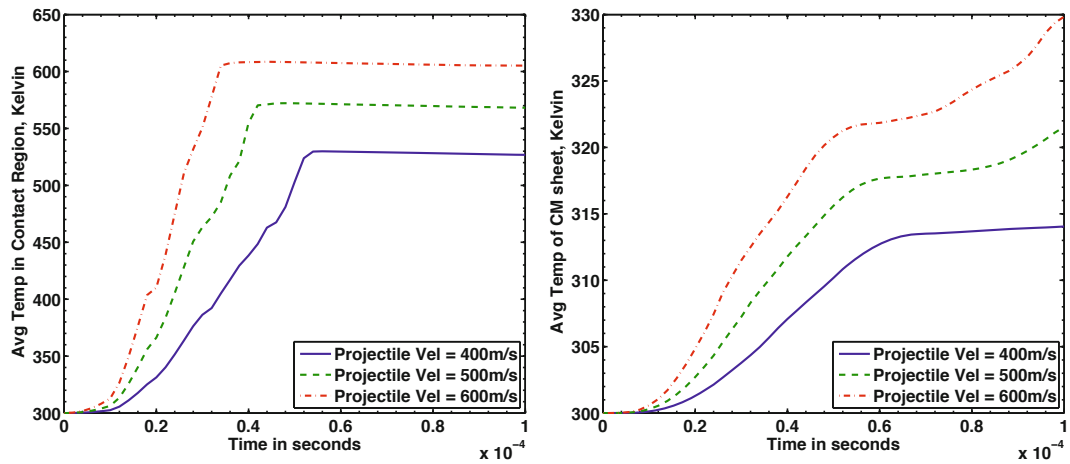

Figure 7: Fixed edge boundary conditions showing the average temperature in the region of contact which is the left plot and the average temperature in the entire CM is the right plot.

defining the thermodynamic response of a CM sheet utilizing a lumped mass model. The general thermodynamic equations were specialized to take advantage of the assumptions made on the CM links. Specifically, that the links are one-dimensional. To allow for the coupling between the thermodynamics and the mechanics, we included viscoplastic effects and assumed a specific form for the plastic flow. The resulting coupled equations are simple and were solved using a staggering scheme. A set of numerical experiments were conducted with various initial projectile velocities. The CM was assumed to fail once a certain value of plastic strain was reached. The two sets of boundary condition used showed that the average temperature of the CM increased with increasing projectile velocity. However, the region of contact was not necessarily the region in which the greatest increase in temperature occurred. In addition, the region of maximum temperature coincides with the region of failure. This is expected since the maximum amount of plastic strain takes place in these regions.

Acknowledgements: This work was funded in part by the Federal Aviation Administration through the Aircraft Catastrophic Failure Prevention Program (cooperative agreement 01-C-AW-UCB and FAA Grant 2007-G-005), the Army Research Laboratory through the Army High Performance Computing Research Center (cooperative agreement W911NF-07-2-0027) and the Powley foundation.

References

[1] Zohdi T.I. Modeling and simulation of progressive penetration of multilayered ballistic fabric shielding. *Computational Mechanics*, 29:61–67, 2002.

[2] Zohdi T.I. and Powell D. Multiscale construction and large-scale simulation of structural fabric undergoing ballistic impact. *Comput. Methods Appls. Mech. Engrg*, 195:94–109, 2006.

[3] Shim V. P. W., Tan V. B. C., and Tay T. E. Modelling deformation and damage characteristics of woven fabric under small projectile impact. *International Journal of Impact Engineering*, 16(4):585–605, August 1995.

[4] Cheeseman B. A. and Bogetti T. A. Ballistic impact into fabric and compliant composite laminates. *Composite Structures*, 61(1-2):161 – 173, 2003. Impact on Composites 2002.

[5] Duan Y., Keefe M., Bogetti T. A., and Cheeseman B. A. Modeling the role of friction during ballistic impact of a high-strength plain-weave fabric. *Composite Structures*, 68(3):331 – 337, 2005.

[6] Duan Y., Keefe M., Bogetti T.A., and Cheeseman B.A. Modeling friction effects on the ballistic impact behavior of a single-ply high-strength fabric. *International Journal of Impact Engineering*, 31(8):996 – 1012, 2005.

[7] Duan Y., Keefe M., Bogetti T.A., and Powers B. Finite element modeling of transverse impact on a ballistic fabric. *International Journal of Mechanical Sciences*, 48(1):33 – 43, 2006.

[8] Tan V.B.C., Shim V.P.W., and Zeng X. Modelling crimp in woven fabrics subjected to ballistic impact. *International Journal of Impact Engineering*, 32(1-4):561 – 574, 2005. Fifth International Symposium on Impact Engineering.

[9] Tabiei A. and Nilakantan G. Ballistic impact of dry woven fabric composites: A review. *Applied Mechanics Reviews*, 61(1):010801, 2008.

[10] Buchholdt H. A., Davies M., and Hussey M.J.L. The analysis of cable nets. *J.Inst. Maths. Applics*, 4:339–358., 1968.

[11] Atai A.A. and Steigmann D.J. On the nonlinear mechanics of discrete networks. *Arch. Appl. Mech*, 67:303–319, 1997.

[12] Atai A.A. and Steigmann D.J. Coupled deformations of elastic curves and surfaces. *Int.J. Solids Struct*, 35:1915–1952, 1998.

[13] Zohdi T.I. A computational framework for network modeling of fibrous biological tissue deformation and rupture. *Computer Methods in Applied Mechanics and Engineering*, 196:2972–2980., 2007.

[14] Park K. C. and Felippa C. A. *Partitioned analysis of coupled systems in: Chapter 3 of Computational Methods for Transient Analysis, ed. by T. Belytschko and T. J. R. Hughes*, pages 821–840. North Holland, Amsterdam, 1983.

[15] Zienkiewicz O. C. *Numerical methods in coupled systems, ed. by R. W. Lewis, P. Bettess and E. Hinton*, chapter Coupled problems and their numerical solution, pages 35–48. Wiley, London, 1984.

[16] Zohdi T. I. and Wriggers P. *An Introduction to Computational Micromechanics*, volume 20. Springer, 2nd edition, 2005.

[17] Zohdi T.I. High-speed impact with electromagnetically sensitive fabric and induced projectile spin. *Computational Mechanics*, 46:399–415, 2010.